ISSN 1068-1620, Russian Journal of Bioorganic Chemistry, 2024, Vol. 50, No. 1, pp. 211–226. © Pleiades Publishing, Ltd., 2024.

Acetylcholine Inhibitory Study of Novel Thio Linked Coumarin-Benzimidazole Derivatives: Design, Synthesis, Computational, and *In Silico* Molecular Docking Studies

T. H. Maruthi Nayaka[a], Itte Pushpavathi[a,*], Pavithra[a], and Y. R. Nagesh[b]

[a] *Department of P.G. Studies and Research in Industrial Chemistry, JnanaSahyadri, Kuvempu University Shankaraghatta, Shivamogga, Karnataka, 577451 India*

[b] *Department of P.G. Studies and Research in Biotechnology, JnanaSahyadri, Kuvempu University Shankaraghatta, Shivamogga, Karnataka, 577451 India*

**e-mail: ittepushpa.chem@gmail.com*

Received August 8, 2023; revised August 20, 2023; accepted August 21, 2023

Abstract—Objective: This article focused on the synthesis and characterization of heterocyclic compounds containing two heteroatoms, as well as computational investigations, the acetylcholinesterase enzyme assay, and antioxidant properties. **Methods:** in this article, we conducted multicomponent reactions and these reactions were based on the condensation method. The DPPH method was used to determine antioxidant activity results. **Results:** The present study includes the synthesis of 3-{[(1-H-benzimidazole-2-yl)sulfanyl](heterocarbaldehyde)methyl}-4-hydroxy-2-*H*-benzopyran-2-one derivatives by the one-pot multicomponent reaction and further structures were characterized by various analytical techniques. **Discussion:** Design and synthesis of coumarin derivatives and confirmed by different spectroscopic techniques DFT calculations at B3YLP/6-311+G(d,p) were used to perform geometry optimization on the coumarin derivatives. MEP provides a visual method for understanding a molecule's reactivity. In Acetylcholinesterase inhibitory assay, the HeLa cell line is treated with synthesized compounds and compounds show promising activity. Additionally, the 3D representation of all derivatives' interactions with proteins and ligands as well as the active site of ligands on receptor surfaces. **Conclusions:** A novel series of coumarin-benzimidazole compounds was successfully developed and synthesized. Among all, compound (**IVa**) demonstrates good inhibition against Hela cancer cell lines, which is corroborated by *in silico* docking studies in which (**IVa**) compound has a good binding affinity of –10.1 kcl/mol, indicating the best binding interactions with the receptor when compared to the target molecules.

Keywords: coumarin-benzimidazole, DFT, molecular docking, acetylcholinesterase

DOI: 10.1134/S1068162024010229

INTRODUCTION

Coumarin is a naturally fragrant and bioactive molecule with a wide range of biological significance, including antibacterial, antifungal, antioxidant, anti-inflammatory, analgesic, herbicidal, and anticancer activity [1–9]. Due to the diversity of bioactivities, coumarin is considered an important scaffold in medicinal and agricultural chemistry [10, 11]. The coumarin derivatives integrating with pyrazole, pyridine, azetidine, and oxazole rings were also discovered to have intriguing antibacterial and antifungal properties [12]. A number of novel coumarin derivatives in combination with triazole pursue effective anticancer activities. It has been discovered that coumarin compounds are useful for photochemotherapy, anticancer, anti-HIV therapy, and inhibitor action. Additionally, coumarin derivatives are finding new uses in material science as laser dyes, nonlinear optical materials, and organic light-emitting diodes [13, 14].

Another important multifaceted nucleus is benzimidazole in the field of medicinal chemistry due to its various pharmaceutical properties. Benzimidazole template is part of many important natural products, such as histidine, purine and vitamin B1. coumarin is an important pharmacophore with high therapeutic potential

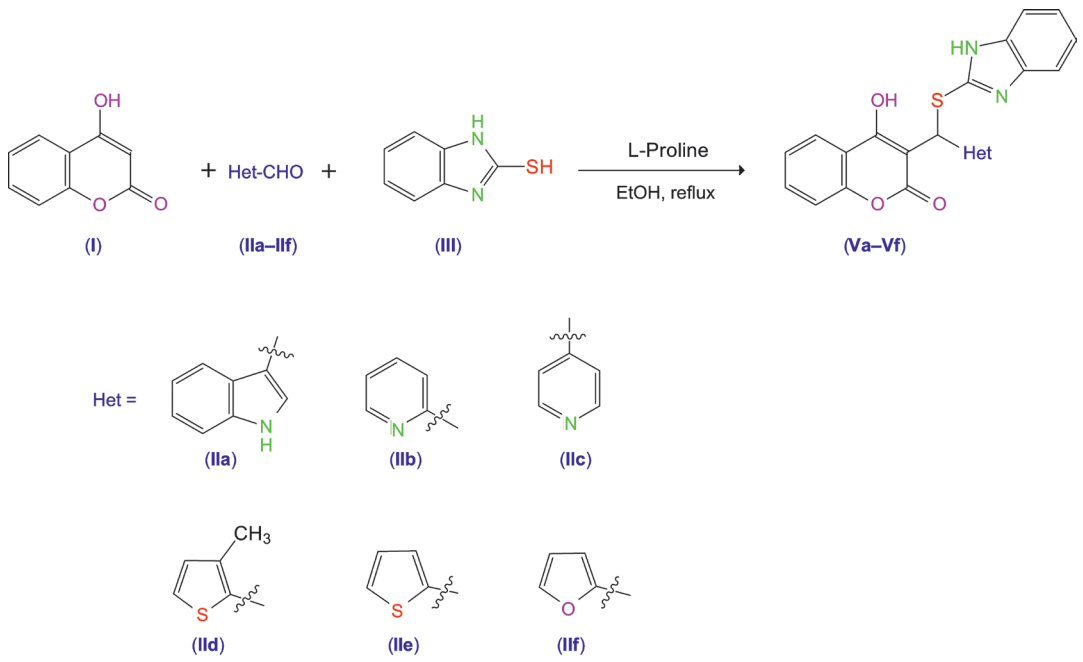

Scheme 1. Synthesis of thioether-linked coumarin-benzimidazole derivatives (**IVa–IVf**).

as an anticancer, anti-inflammatory, antihypertensive, antiprotozoal, anthelmintic, antiviral and antitubercular medication [15].

The presence of one or more pharmacophores with diverse biological activities such as coumarin and benzimidazole improves efficacy and reduces the toxicity of the synthesized hybrid molecules [16, 17]. Owing to the compelling biological significance of coumarin derivatives in pharmaceutical chemistry and drug discovery leads us to synthesize a novel series of coumarin derivatives.

One pot synthesis is a fast solution for the formation of pharmaceutically important products with high atom economy. Therefore, in a quest for a novel agent, we design a one-pot synthesis of coumarin-benzimidazole derivatives while taking into account the structure-activity relationship at the active side [18, 19], which we design, a multi-component reaction for the formation of coumarin derivatives and further confirmation were carried out by IR, NMR, LC-MS, and elemental analysis. As computational analysis is of current interest in the field of synthetic organic chemistry, it encouraged us to perform DFT studies to analyse the structural properties, global parameters, Non-linear optical (NLO) properties and thermodynamic properties of the resulting derivatives. In addition, *in silico* molecular docking is performed to investigate receptor docking interactions on target molecules [20–22].

RESULTS AND DISCUSSION

Chemistry

The present study includes the synthesis of 3-{[(1-*H*-benzimidazole-2-yl)sulfanyl](heterocarbaldehyde)-methyl}-4-hydroxy-2-*H*-benzopyran-2-onederivatives (**IVa–IVf**) by the one-pot multicomponent reaction of 4-Hydroxycoumarin (**I**), heterocyclic aldehyde (**IIa–IIf**), and 2-mercaptobenzimidazole (**III**) using L-proline as a catalyst. The synthetic route is shown in Scheme 1 and further structures were characterized by various analytical techniques.

Computational Study

DFT calculations at B3YLP/6-311+G(d,p) were used to perform geometry optimization on the coumarin derivatives (**IVa–IVf),** and the resulting structures are shown in the supplementary information (Fig. S1, see Supplementary Information). The optimized structures' stability (minimal energy) is confirmed by the wave numbers analysis at the same basis set level, and all the compounds displayed C1 symmetry. In comparative

studies, theoretical IR and NMR data are compared with experimental data and both are in close agreement.

IR Spectral Analysis

The characteristic stretching and bending vibrations of the target compounds (**IVa–IVf**) between 4000 and 500 cm^{-1} have been studied using FT-IR spectroscopy. The theoretical frequencies and intensities of the derivatives are calculated using the vibrational analysis, which is carried out by DFT at the B3YLP/6-311+G(d,p) basis set in the gas phase. The number of atoms in the synthesized compounds (**IVa–IVf**) is 49, 44, 44, 45, 42, and 42, and their respective non-linear (3N-6) fundamental modes of vibration are 141, 126, 120, and 120. To reduce the overestimation of vibrational modes caused by the neglect of anharmonicity, the vibrational frequencies were scaled using the scaling factor 0.967 of the corresponding basis set, and the molecules (**IVa**), (**IVb**), (**IVd**), (**IVe**), and (**IVf**) of the IR spectra are displayed in Figs. S2–S6 of the supplementary information.

The experimental values were compared with the theoretical scaled frequencies(DFT) for the synthesized compounds (**IVa–IVf**) which are shown in Tables S1–S6 of the supplementary information. In the FT-IR spectrum, Slight deviations might be observed as the computational vibrational analysis (DFT) was conducted in the gas phase whereas FT-IR analysis was in the solid phase [23].

O–H Vibrations

The experimentally determined O–H stretching frequencies for the coumarin derivatives (**IVa–IVf**) are observed at 3426, 3428, 3430, 3413, 3428, and 3441cm^{-1}, respectively, whereas DFT values were shown at 3653, 3800, 3652, 3652, 3652, and 3633cm^{-1}.

N–H Vibrations

For all synthesized derivatives (**IVa–IVf**), the N–H stretching bands appeared at 3166, 3080, 3089, 3081, 3077, and 3094 cm^{-1} in FT-IR and the theoretically predicted peaks were found at 3200, 3233, 3208, 3236, 3237, and 3280 cm^{-1}.

C=O Vibrations

The characteristic carbonyl stretching frequency of all derivatives (**IVa–IVf**) were observed at 1679, 1657, 1659, 1668, 1672, and 1676 cm^{-1} respectively and theoretically calculated peaks occurred at 1760, 1665, 1668, 1760, 1760, and 1680 cm^{-1} respectively.

C=N Vibrations

The experimental obtained C=N stretching bands for coumarin derivatives (**IVa–IVf**) appeared at 1570, 1563, 1573, 1563, 1577, and 1576 cm^{-1} and DFT analysis exhibits peaks at 1590, 1601, 1598, 1592, 1592, and 1605 cm^{-1}.

^{1}H NMR and ^{13}C NMR Spectral Data

NMR spectroscopy is a key tool to confirm the structure of organic compounds. In DMSO-d_6, the ^{1}H and ^{13}C NMR spectra of synthesized compounds (**IVa**), (**IVb**), (**IVd**), (**IVe**), and (**IVf**) were recorded and given in Figs. S7–S11 (supplementary information).

The CH (aliphatic) junction proton reverberated as a singlet at 5.86–6.44 ppm in the ^{1}H NMR spectra of compounds (**IVa–IVf**), while the aromatic protons produced as a multiplet in the range 6.35–8.08 at 9.18–12.58 ppm, the imidazole ring NH proton was visible as a singlet.

In these derivatives' ^{1}H NMR spectra, there are no OH signals from protons linked to coumarin, which may be explained by interactions with the solvent DMSO-d_6 [24–26] (Table 1).

In ^{13}C NMR spectra, aromatic carbons resonated between 115 and 164 ppm, junction C–S group resonated between 35.75 and 36.38 ppm, and carbonyl (C=O) carbon resonated between 165.46 and 167.22 ppm, as seen in Figs. S12– S14. But woefully, the ^{13}C NMR of compounds (**IVc**) and (**IVd**) were not recorded due to their low solubility in DMSO. By using the Gauge-Independent Atomic Orbital (GIAO) approach at B3LYP/6-311+G(d,p), the theoretical ^{1}H NMR spectra were calculated. The experimental chemical shift values, the theoretically estimated NMR values, and the suggested structures agreed quite closely. Experimental and theoretical ^{1}H NMR values of compound (**IVa**) are provided in Table S1 and for other derivatives (**IVb–IVf**) given supplementary information.

Mass Spectra

The synthesized compound's mass spectra were recorded, and the molecular ion peaks of synthesized molecules observed were found at *m/z* 439.19, 401.17,

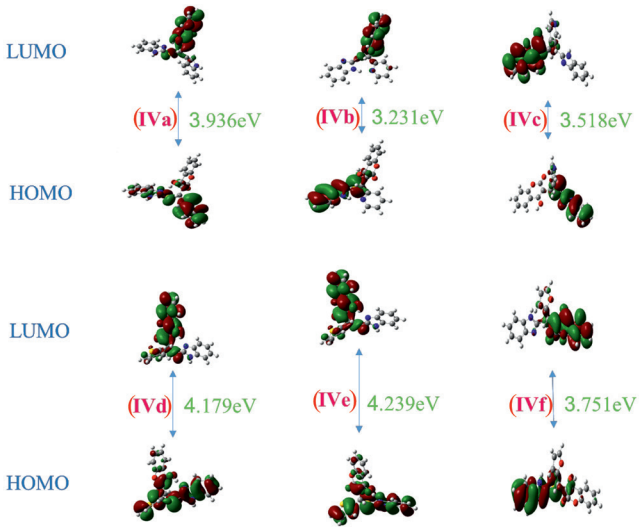

Fig. 1. 3D representation of FMO orbitals and HOMO-LUMO energy gap of the synthesized compounds (**IVa–IVf**).

401.30, 420.70, 407.10, and 390.48, respectively, correlating to their molecular masses. Mass spectra of (**IVa**), (**IVb**), (**IVd**) and (**IVf**) are given in supplementary information in Figs. S15–S18.

DFT Studies

The main aim of computational studies includes the geometry optimization, calculation of global parameters, MEP and nonlinear optical properties to study the reactivity of the synthesized compounds. Analysis of thermodynamic properties and correlation graphs predicted to explain, the temperature depending nature of synthesized compounds.

Table 1. Experimental theoretical ^{1}H NMR values of compound (**IVa**)

H-atoms	^{1}H NMR	
	theoretical	experimental
H33	8.517	7.988
H34	7.523	7.408
H35	7.589	7.606
H36	7.868	7.929
H37	14.896	–
H38	7.087	6.449
H39	8.293	12.589
H40	8.01	7.949
H41	7.518	7.388
H42	7.572	7.592
H43	7.456	–
H44	8.027	12.589
H45	8.818	8.085
H46	7.835	7.644
H47	7.343	7.326
H48	7.634	7.625
H49	7.458	7.345

HOMO-LUMO Analysis

The energies of the Frontier orbitals, HOMO and LUMO, and their band gap, were calculated using the DFT method using the B3LYP/6-311+G(d,p) basis set. In addition, global parameters including electronegativity, electron affinity, ionization energy, electrophilicity index, hardness, softness, and chemical potential were determined and summarized in Table 2. We explore the chemical reactivity and stability of molecules as a result of the energy difference between HOMO and LUMO [27, 28]. When the energy gap is small and the molecule is seen to be soft, a molecule is said to be more polar and reactive, and when the gap is high, the molecule is thought to be hard and stable [29].

$$\text{Electronegativity } (\chi) = (I + A)/2;$$

$$\text{Global hardness } (\eta) = (I - A)/2;$$

$$\text{Chemical potential } (\mu) = -(I + A)/2;$$

$$\text{Global softness } (S) = 1/2\eta;$$

$$\text{Electrophilicity index } (\omega) = \mu^2/2\eta.$$

According to the HOMO-LUMO diagram in Fig. 1, the electron density in HOMO orbitals is primarily dispersed in the benzimidazole and indole rings, whereas in LUMO, the electron density is primarily

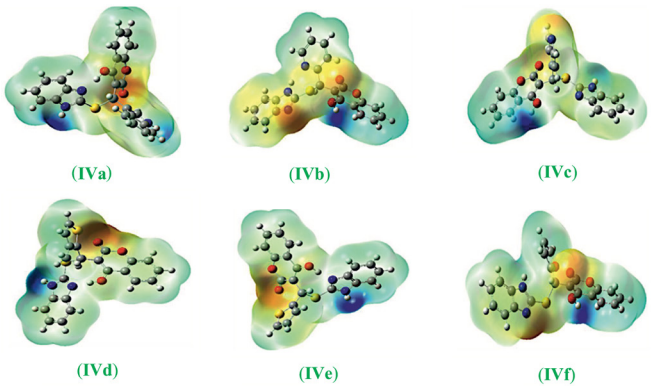

Fig. 2. The molecular electrostatic potential surface of synthesized molecules (**IVa–IVf**).

distributed in the coumarin ring. Among all compounds, compound (**IVe**) has the largest energy gap (4.29 eV), whereas compound (**IVb**) has the smallest energy gap (3.23 eV). The intramolecular electron transfer from the benzimidazole ring (HOMO) to the coumarin ring (LUMO) is accomplished by all compounds (**IVa–IVf**) exhibiting a smaller band gap in the range 3.23–4.34eV.

Molecular Electrostatic Potential Map (MEP)

The charge distribution of a molecule's electrophilic and nucleophilic sites is represented in three dimensions by electrostatic potential surfaces [30]. MEP provides a visual method for understanding a molecule's reactivity. The negative ESP is due to nucleophilic sites (electron rich centres) appeared in red shades and the positive ESP is due to the electrophilic sites (electron deficient centres) appear in blue shades. The neutral sites are illustrated by green shades. The potential increases in the order of colors as red<orange<yellow<green<blue. All of the target molecule's electrostatic potential energy maps were computed by B3YLP/6-311+G(d,p), and the MEP diagram of these compounds is shown in Fig. 2. From the MEP diagram, it can be seen that the NH group of the imidazole ring and the OH group connected to coumarin have a larger positive electrostatic potential, which is indicated by the blue color. While the remainder of the molecular structures has zero electrostatic potential, the higher negative electrostatic potential is seen in red over the carbonyl group in coumarin and green over the heterocyclic ring linked to the hydrogen atoms of all the compounds.

Non-Linear Optical Properties

Due to its numerous applications such as frequency shifting, and optical memory in the fields of telecommunications, signal processing, and optical interconnection technologies, non-linear optical property is significant in current research. NLO study includes the interaction of intense electromagnetic fields with various media to produce different fields with changes in amplitude, phase, and frequency. The synthetic organic compounds with π conjugation were studied for their non-linear properties [31]. The non-linear parameters μ_α, α and β_0 are the components of dipole moment, polarizability, and the first hyperpolarizabilities, respectively calculated in the DFT method at B3YLP/6-311+G(d,p) basis set. These values μ, α, Δα, and β_0 using the x, y, and z components are defined as follows:

Table 2. The global parameters and energies HOMO and LUMO of the synthesized compounds (**IVa–IVf**)

Parameters	(IVa)	(IVb)	(IVc)	(IVd)	(IVe)	(IVf)
E_{HOMO} (eV)	–5.761	–5.688	–5.920	–6.101	–6.177	–5.935
E_{LUMO} (eV)	–1.825	–2.456	–2.402	–1.921	–1.937	–2.184
Energy gap (Δ) (eV)	3.936	3.231	3.518	4.179	4.239	3.751
Ionization energy (I) (eV)	5.761	5.688	5.920	6.101	6.177	5.935
Electron affinity (A) (eV)	1.825	2.456	2.402	1.921	1.937	2.184
Electronegativity (χ) (eV)	3.793	4.072	4.161	4.011	4.057	4.059
Chemical potential (μ) (eV)	–3.793	–4.072	–4.161	–4.011	–4.057	–4.059
Global hardness (η) (eV)	1.968	1.616	1.759	2.09	2.12	1.875
Global softness (S) (eV^{-1})	0.253	0.309	0.316	0.239	0.235	0.266
Electrophilicity index (ω) (eV)	3.654	5.129	4.921	3.848	3.881	4.393

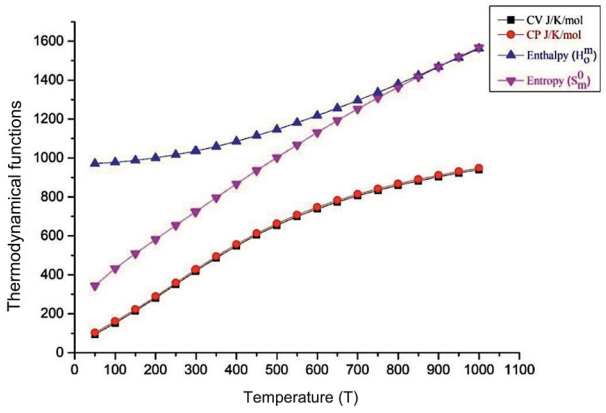

Fig. 3. Correlation graphs of thermodynamic properties at different temperatures for the synthesized compound (**IVa**).

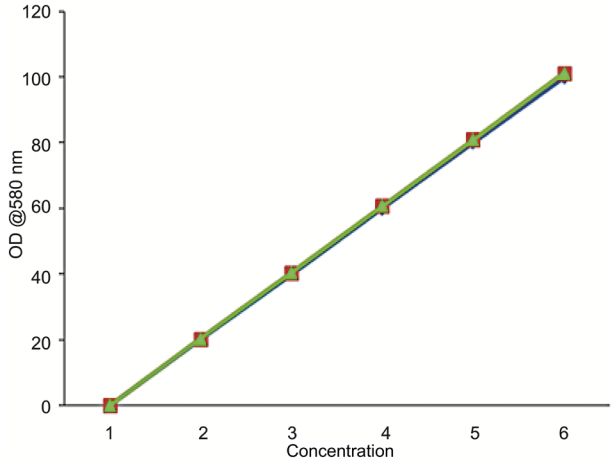

Fig. 4. The standard graph of acetyl CoA synthesized compounds (**IVa–IVf**).

$$\mu = (\mu^2_x + \mu^2_y + \mu^2_z)^{1/2}, \quad (1)$$

$$\alpha = (\alpha_{xx} + \alpha_{yy} + \alpha_{zz})/3, \quad (2)$$

$$\Delta\alpha = 2^{-1/2}[(\alpha_{xx} - \alpha_{yy})^2 + (\alpha_{yy} - \alpha_{zz})^2 + (\alpha_{xx} - \alpha_{zz})^2 + 6\alpha^2_{xx}]^{1/2}, \quad (3)$$

$$\beta_0 = (\beta^2_x + \beta^2_y + \beta^2_z)^{1/2}; \quad (4)$$

here,

$$\beta_x = \beta_{xxx} + \beta_{xyy} + \beta_{xzz},$$

$$\beta_y = \beta_{yyy} + \beta_{xxy} + \beta_{yzz},$$

$$\beta_z = \beta_{zzz} + \beta_{xxz} + \beta_{yyz}.$$

In Table 3, the estimated parameters are listed. Urea is considered a prototype molecule ($\beta_0 = 0.372 \times 10^{-30}$) in NLO properties of molecular systems for comparative investigations. The synthetic molecules (**IVa**), (**IVc**), and (**IVf**) have hyperpolarizability (β_0) values that are seven times higher than those of urea, indicating a stronger NLO characteristic. Due to their high polarizability, these molecules will therefore be thought of as NLO in the future. The dipole moment is an important parameter to determine molecular stability in the polar environment [32, 33]. Among the synthesized compounds (**IVb**) has a high dipole moment (9.4681 Debye) due to higher dipole interaction.

Thermodynamic Properties

Thermodynamic characteristics were computed at various temperatures to investigate the temperature dependence of the target compounds. With the aid of MOLTRAN software, standard thermodynamic quantities such as specific heat capacity (C_P and C_V), internal energy, enthalpy, and entropy were calculated in the temperature range (100–1000 K), and a correlation graph was plotted for compound (**IVa**) in Fig. 3. The correlation graph of (**IVb–IVf**) compounds is provided in the supplementary information (Fig. S18). Due to an increase in molecular vibrations, as temperature rises, it has been observed that the values of C_P, C_V, U, H, and S increase as temperature increases from 100 to 1000 K. Based on the second rule of thermodynamics and the thermochemical field, this thermodynamic data can be used to calculate other thermodynamic energies and identify chemical reaction directions [34, 35].

Biological Studies
Acetylcholinesterase Inhibitory Assay

In Acetylcholinesterase inhibitory assay, the HeLa cell line is treated with synthesized compounds (**IVa–IVf**) related to their Acetyl-CoA inhibitory activity at varying concentrations (10 to 50 µg/mL). Table 4 presents the findings with the percentage of (**IVa–IVf**) compounds that inhibit Acetyl-CoA. Due to the presence of indole moiety, ligand (**IVa**) demonstrates significant activity with 19.09 µg/mL, ligands, (**IVb**) and (**IVc**) have good activity due to the presence of the pyridine moiety, while ligands (**IVe**) and (**IVf**) have a moderate degree of activity, while ligand (**IVd**) molecule has a lower activity of 40.4 µg/mL. Figure 4 depicts the Acetyl-CoA standard graph and activity images of the synthetic compounds.

Table 3. Dipole moment μ (Debye), polarizability α (esu), mean polarizability Δα (esu), β components and first-order hyperpolarizability β_0 (esu) value of title molecule calculated at B3LYP/6-311G+(d,p)

(**IVa**)		(**IVb**)		(**IVc**)	
parameters	values	parameters	values	parameters	values
μ_x	–1.8508	μ_x	6.0512	μ_x	–3.1383
μ_y	–0.9258	μ_y	1.2679	μ_y	–5.5866
μ_z	0.0810	μ_z	–7.1708	μ_z	1.6644
μ	2.071	μ	9.4681	μ	6.6204
α_{xx}	–164.5355	α_{xx}	–153.8752	α_{xx}	–141.7469
α_{xy}	–1.6499	α_{xy}	–19.4223	α_{xy}	12.2338
α_{yy}	–175.7788	α_{yy}	–154.9753	α_{yy}	–189.6449
α_{xz}	4.7330	α_{xz}	–1.6889	α_{xz}	–17.3681
α_{yz}	12.7758	α_{yz}	1.5722	α_{yz}	–9.5968
α_{zz}	–191.6375	α_{zz}	–180.7459	α_{zz}	–165.1598
α (au)	177.3172	α (au)	–111.5403	α (au)	–496.5523
α (esu)	26.278×10^{-24}	α (esu)	-16.53×10^{-24}	α (esu)	73.589×10^{-24}
$\Delta\alpha_a$ (au)	285.9553	$\Delta\alpha_a$ (au)	267.8152	$\Delta\alpha_a$ (au)	248.8981
$\Delta\alpha_a$ (esu)	40.84×10^{-24}	$\Delta\alpha_a$ (esu)	39.69×10^{-24}	$\Delta\alpha_a$ (esu)	36.887×10^{-24}
β_{xxx}	–5.8254	β_{xxx}	190.4753	β_{xxx}	–125.3810
β_{xxy}	–84.0667	β_{xxy}	–68.6919	β_{xxy}	–101.7753
β_{xyy}	75.1888	β_{xyy}	29.0672	β_{xyy}	–50.2309
β_{yyy}	109.4914	β_{yyy}	103.8650	β_{yyy}	–87.2463
β_{xxz}	–50.2699	β_{xxz}	–50.6636	β_{xxz}	–23.3107
β_{xyz}	–9.7002	β_{xyz}	27.0526	β_{xyz}	18.3693
β_{yyz}	22.7167	β_{yyz}	–35.1175	β_{yyz}	–22.7140
β_{xzz}	–56.3716	β_{xzz}	–56.3716	β_{xzz}	33.8256
β_{yzz}	–20.1698	β_{yzz}	–24.0280	β_{yzz}	–35.1086
β_{zzz}	–8.8603	β_{zzz}	–43.1987	β_{zzz}	25.9038
β_0 (au)	39.0168	β_0 (au)	268.6194	β_0 (au)	265.9711
β_0 (esu)	0.3371×10^{-30}	β_0 (esu)	2.321×10^{-30}	β_0 (esu)	2.298×10^{-30}

Since the values of the polarizabilities (α) and first-order hyperpolarizability (β) of GAUSSIAN-09W output are in atomic units (a.u.), and converted into electrostatic units (esu). A : 1 a.u. = $0.1482 \times 10–^{24}$ esu; β : 1 a.u. = 8.6393×10^{-33} esu).

Table 4. Acetylcholinesterase inhibitory assay of the synthesized compounds (**IVa–IVf**)

Compound	IC_{50} values (μg/mL)
(**IVa**)	19.09
(**IVb**)	24.72
(**IVc**)	29.1
(**IVd**)	40.4
(**IVe**)	34.2
(**IVf**)	34.2

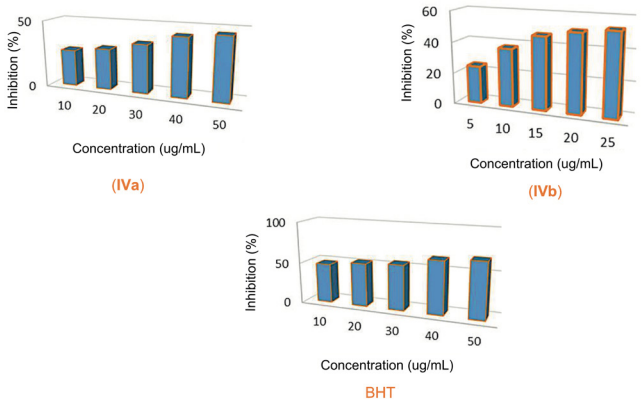

Fig. 5. Standard graph DPPH radical assay of (**IVa**), (**IVb**) compounds and standard drug BHT.

DPPH Free Radical Scavenging Assay

The discovery of natural or synthetic antioxidants is important to prevent the organism from being damaged by free radicals [36]. The DPPH radical scavenging assay was used to test the antioxidant activity of the recently synthesized compounds (**IVa–IVf).** In Table 5, the findings of an analysis of the stable 2,2-diphenyl-1-pecrylhydrazyl (DPPH) radical scavenging activity of target compounds at different concentrations and the standard butylated hydroxytoluene (BHT) are presented. Compound (**IVb**) has the strongest inhibitions compared to the reference (BHT), with an IC_{50} value of 20.46 mg/mL. while, compounds (**IVc**), (**IVe**), and (**IVf**) offered better inhibition with IC_{50} –36.34, 35.84, 37.99, and 39.27 mg/mL respectively and the remaining compounds exhibited lesser inhibition. Figure 5 provides a standard graph for the DPPH radical assay of (**IVa**), (**IVb**) chemicals and the reference medication BHT. The scavenging radical inhibition also rises with the sample concentration, which lowers the IC_{50} value. This suggests that the (**IVb**) material has a better capacity for scavenging DPPH, which also suggests a higher level of antioxidant activity [37, 38].

Drug-Likeness Properties

The Molinspiration web tool is used to virtually screen molecules with the highest likelihood in order to explore the pharmacokinetics and drug-like features of the target compounds. Table 6 lists the values for molecular characteristics, including the partition coefficient (logP), molecular weight (MW), number of rotatable bonds, number of hydrogen bond acceptors, and number of hydrogen bond donors. It was noted that the synthetic compounds (**IVa**), (**IVc**), and (**IVf**) adhere to Lipinski's rule of five with no violations, while the remaining compounds (**IVa**), (**IVd**), and (**IVe**) with one violation [39]. A very good descriptor for understanding drug absorption, including intestinal absorption, bioavailability, and blood-brain barrier penetration, is the topological polar surface area (TPSA) parameter, which is evaluated to analyse drug transport properties of molecules and is found in the range of 79.12–94.12 (140) [40, 41].

The bioactive characteristics used to assess a molecule's potential for drug development, such as GPCR, ion channel modulator, kinase inhibitor, nuclear receptor ligands, protease inhibitor, and enzyme inhibitor, were compiled in Table 7. A chemical is thought to be more

Table 5. DPPH radical scavenging assay of the synthesized compounds (**IVa–IVf**)

Compound	IC_{50} values
(**IVa**)[a]	56.38 (0.05 mg/2 mL)
(**IVb**)	20.46 (5 mg/2.5 mL)
(**IVc**)	36.34 (5 mg/2.5 mL)
(**IVd**)[a]	88.34 (0.05 mg/2 mL)
(**IVe**)	35.84 (5 mg/2.5 mL)
(**IVf**)	37.99 (5 mg/2.5 mL)
BHT	15.45 (5 mg/2.5 mL)

[a] (**IVa**) and (**IVf**) samples were taken in 0.05 mg (50 µg/2 mL) due to the coloring nature and the rest of the samples were taken as 5 mg/2.5 mL

Table 6. Drug-likeness of synthesized compounds (**IVa–IVf**)

Compound	Lipinski rule								
	M W	LogP	TPSA	*n*-atoms	*n*-ON	*n*-OHNH	*n*-violations	*n*-rotb	volume
(**IVa**)	439.50	5.39	94.12	32	6	3	1	4	368.18
(**IVb**)	401.45	4.07	92.01	29	6	2	0	4	335.04
(**IVc**)	401.45	3.95	92.01	29	6	2	0	4	335.04
(**IVd**)	420.51	5.51	79.12	29	5	2	1	4	346.47
(**IVe**)	406.49	5.14	79.12	28	5	2	1	4	329.91
(**IVf**)	390.42	4.49	92.26	28	6	2	0	4	320.77

Table 7. Bioactive score of synthesized compounds (**IVa–IVf**)

Compound	Bioactivity score					
	GPCR ligand	ion channel modulator	kinase inhibitor	nuclear receptor ligand	protease inhibitor	enzyme inhibitor
(**IVa**)	–0.25	–0.31	–0.24	–0.49	–0.25	0.03
(**IVb**)	–0.25	–0.17	–0.25	–0.48	–0.26	0.06
(**IVc**)	–0.37	–0.35	–0.30	–0.66	–0.29	0.01
(**IVd**)	–0.46	–0.51	–0.47	–0.64	–0.49	–0.16
(**IVe**)	–0.45	–0.50	–0.44	–0.64	–0.44	–0.13
(**IVf**)	–0.41	–0.47	–0.47	–0.62	–0.47	–0.13

Table 8. Findings of docking studies of the designed molecules against 1W6R

Molecules	Affinity (kcal/mol)	H-bonds	H-bond length (Å)	H-bond with residue	Hydrophobic interactions
(**IVa**)	–10.1	3	2.12 2.90 3.30	Tyr-70 Tyr-121 Asp-72	Tyr-70, Asp-237, Tyr-70, Phe-330, Phe-331, Tyr-121, Tyr-334, Ile-287, Phe-288, Arg-289, Asp-72, Phe-290, Trp-279, Prc-86, Trp-84
(**IVb**)	–8.3	3	2.50 2.30 2.60	Arg-289 Arg-289 Arg-289	Arg-289, Ser-237, Glu-240, Arg-244, Arg-289, Arg-289, Pro-283, Phe-284, Pro-361, His-362, Arg-289, Leu-532, Pro-232
(**IVc**)	–10.1	1	2.70	Tyr-121	Tyr-121, Gly-123, Gly-119, Gly-141, His-440, Tyr-121, Ser-122, Trp-84, Gln-69, Asn-85, Pro-86, Ser-81, Tyr-70, Asp-72, Tyr-334, Trp-279, Phe-331, Phe-330, Phe-290, Phe-288
(**IVd**)	–7.9	2	2.10 3.40	Asn-230 Asn-525	Asn-230, Glu-306, Leu-305, Ser-304, Asn-525, His-406, Asn-525, Pro-403, Asn-230, Cys-231, Pro-232, His-398, Ser-235
(**IVe**)	–7.9	3	2.60 2.44 2.44	Glu-306 Glu-306 Asn-230	Glu-306, Leu-305, Pro-229, Asn-230, Glu-306, Ser-235, Cys-231, Pro-232, His-406, Asn-230, Asn-525, Pro-529, Trp-524, His-396, Asp-397
(**IVf**)	–7.8	1	2.70	Ser-286	Ser-286, Tyr-334, Phe-331, Gln-74, Asp-72, Tyr-70, Ile-287, Ser-286, Phe-288, Arg-289, Leu-282, Phe-290, Trp-279, Tyr-12
Docetaxel	–6.3	3	2.20 2.80 2.30	– – –	Glu-299, Phe-300, Ser-212, Pro-213, Gly-24, Leu-171, Ser-215, Leu-171, Met-175, Gcn-178, Pro-48, Arg-47, Gly-214, Arg-47, Arg-174, Leu-218, Arg-47

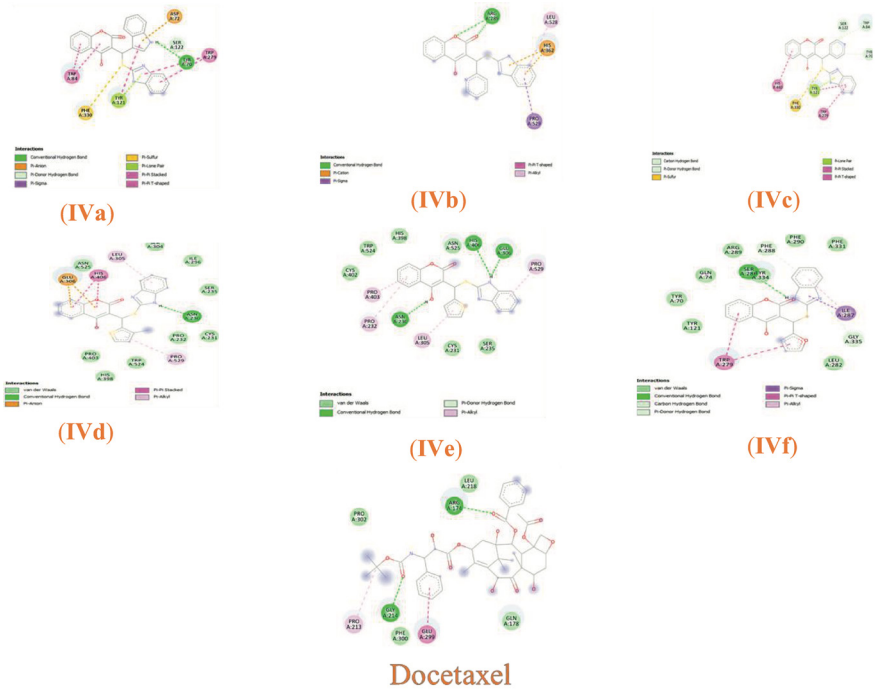

Fig. 6. 2D diagrams of molecular interaction (**IVa–IVf**) with residues of receptors and standard drug Docetaxel.

bioactive if its bioactive score is greater than 0.00, moderately active if it is between –0.50 and 0.00, and inert if it is below –0.50. Table 7 of the results suggests that all target compounds have a moderate level of bioactivity [42].

Molecular Docking Studies

Molecular docking research is critical in the fields of computer-aided drug design and pharmacogenomics. It is a computer-based program that studies the interactions of ligands (synthesized compounds) with specific receptors [43, 44]. All of the synthesized compounds were docked using the acetylcholinesterase enzyme receptor 1W6R, and the docking results were given in Table 8. The table provides information about the number of hydrogen bonds, interacting residues, hydrophobic interactions, and binding affinities. According to the findings, the receptor (1W6R) and the ligand molecules (**IVa–IVf**) demonstrate a significant number of hydrogen bonds and a greater number of hydrophobic contacts. Molecules (**IVa**) and (**IVc**) have a greater binding affinity of –10.1 kcal/mol compared to the other synthesized compounds. The presence of an indole ring in compound (**IVa**) is a response for enhanced activity and best binding affinity which is supported by the experimental acetyl-CoA inhibition studies in which (**IVa**) demonstrates significant activity. Compound (**IVb**) has a moderate binding affinity of –8.3 kcal/mol, and (**IVf**) has a lower binding affinity of –7.8 kcal/mol. As a result, all of the recently synthesized compounds demonstrate good binding affinity in the range of –7.8 to –10.1 kcal/mol when compared to the standard drug Docetaxel, whose binding affinity is –6.03 kcal/mol. Figures 6 and 7 show the 3D and 2D diagrams of ligand molecules' interactions with receptor residues respectively. Additionally, the 3D representation of all derivatives' interactions with proteins and ligands as well as the active site of ligands on receptor surfaces are given in supplementary information (Figs. S19, S20).

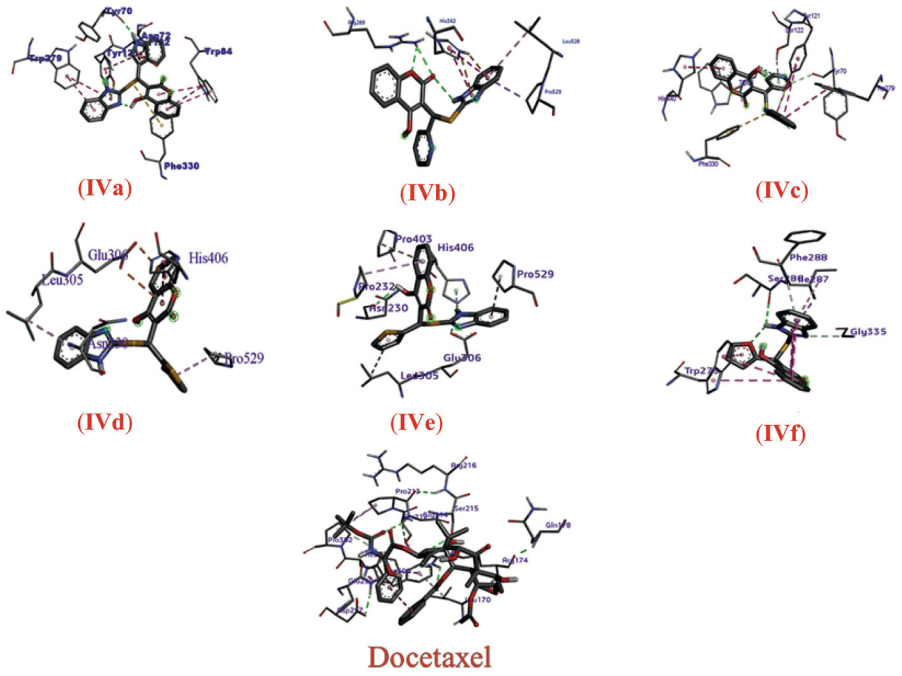

Fig. 7. 3D diagrams of molecular interaction (**IVa–IVf**) with residues of protein and standard drug Docetaxel.

EXPERIMENTAL

Materials and equipment. All the chemicals and solvents are purchased from Sigma Aldrich, Indian Mart and used further without purification. Thin-layer chromatography (TLC) is used for confirmation of reaction completion and melting points were measured in an electrothermal apparatus. IR spectra were recorded on a Jasco 6300 FT-IR spectrometer. ^{1}H and ^{13}C NMR recorded in DMSO-d_6 with vnmrs 400 instrument.

Computational methodology. All computational calculations. All Density functional theory (DFT)-based computer calculations were done on Gaussian 09W software. The theoretical properties of the synthesized compounds were studied through optimization using the hybrid Becke 3 Lee-Yang-Parr correlation functional with the basis set B3LYP/6-311+G(d,p). At the same gas phase basis set level, the normal mode frequency analysis was performed. The Gauge-Independent Atomic Orbital (GIAO) approach was chosen to predict NMR spectra at the B3LYP/6-311+G(d,p) basis set in the solvent phase (DMSO) [45–47]. The thermodynamic parameters, global parameters, and nonlinear optical properties were estimated at the same theoretical level.

General procedure for the synthesis of 3-(((benzo[*d*]-imidazole-2yl)thio)(heterocarbaldehyde)methyl)-4-hydroxynaphthalen-2(1*H*)-one derivatives (IVa–IVf). A mixture of substitute heterocyclic aldehydes, 4-hydroxy coumarin, and 2-mercapto benzimidazole was added to a 50 mL round bottom flask along with 20 mL of ethanol to make an equimolar (1 mmol) solution. L-proline (10 mol %) was added to the mixture and refluxed for roughly 8 h at 70°C. TLC plates were used to track the reaction's progress moving forward. A solid product was precipitated and dried with absolute ethanol and the final product was obtained by recrystallizing a solid product with hot methanol.

3-(((Benzo[*d*]imidazole-2yl)thio)(1*H*-indol-3-yl)-methyl)-4-hydroxynaphthalen-2(1*H*)-one (IVa). Brown

solid; yield: 78%; mp 138–140°C; FT-IR (KBr) ν_{max}, cm^{-1}: 3426.49 (–OH), 3166.29 (N–H), 2840.48 (Ar–C–H), 1679.57 (C=O), 1570.84 (C=N), 1461.46 (C=C), 760.13 (C–S), ^{1}H NMR (400 MHz, DMSO-d_6), ppm: 12.6 (s, 2H, NH), 8.08–8.06 (d, 1H, J = 7.6 Hz, Ar–H), 7.98–7.92 (t, 3H, J = 8 Hz, Ar–H), 7.70–7.68 (d, 1H, J = 7.6 Hz, Ar–H), 7.647.55 (m, 3H, Ar–H), 7.40–7.32 (m, 4H, Ar–H), 6.44 (s, 1H, CH); ^{13}C NMR (100 MHz, DMSO-d_6), ppm: 164.44 (C=O), 152.44, 147.89, 143.84, 134.06, 131.94, 129.58, 124.08, 123.66, 121.33, 120.80, 118.41, 116.0, 103.36 (CH), 36.38 (C-S Junction); LC-MS: *m/z* 439.19 [M^+]; $C_{25}H_{17}N_3O_3S$; Calculated, %: C, 68.32; H, 3.90; N, 9.56; O, 10.92; S, 7.30; Found, %: C, 68.35; H, 3.8; N, 9.60; O, 10.86; S, 7.32.

3-(((Benzo[*d*]imidazole-2yl)thio)(pyridine-2-yl)-methyl)-4-hydroxynaphthalen-2(1*H*)-one (IVb). White solid; yield: 76%, mp 122–124°C; FT-IR (KBr) ν_{max}, cm^{-1}: 3428.58 (–OH), 3080.42 (N–H), 2924.95 (Ar–H), 1657.90 (C=O), 1563.20 (C=N), 1445.55 (C=C), 763.19 (C–S); ^{1}H NMR (400 MHz, DMSO-d_6), ppm: 9.18 (s, 1H, NH), 7.95–7.93 (t, 2H, J = 6.8 Hz, Ar–H), 7.62–7.60 (d, 2H, J = 8.4 Hz, Ar–H), 7.20–7.40 (m, 7H, Ar–H), 6.37 (s, 1H, CH), ^{13}C NMR (100 MHz, DMSO-d_6), ppm: 165.46 (C=O), 164.71, 152.27, 139.29, 131.97, 130.14, 128.74, 127.96, 123.95, 123.77, 117.95, 115.99, 103.92 (CH), 35.71 (C-S Junction); LC-MS: *m/z* 401.17 [M^+]; $C_{22}H_{15}N_3O_3S$; Calculated, %: C, 68.32; H, 3.90; N, 9.56; O, 10.92; S, 7.30; Found, %: C, 68.26; H, 3.94; N, 9.55; O, 10.97; S, 7.28.

3-(((Benzo[*d*]imidazole-2yl)thio)(pyridine-4-yl)-methyl)-4-hydroxynaphthalen-2(1*H*)-one (IVc). White solid; yield: 80%, mp 118–120°C; FT-IR (KBr) ν_{max}, cm^{-1}: 3430.48 (–OH) 3089.27 (N–H), 2934.22 (Ar–H), 1659.49 (C=O), 1573.50 (C=N), 1448.64 (C=C), 768.15 (C–S); ^{1}H NMR (400 MHz, DMSO-d_6), ppm: 9.24 (s,1H, NH), 7.94–7.92 (m, 3H, Ar–H), 7.61–7.59 (d, 2H, J = 8 Hz, Ar–H), 7.52–7.25 (m, 7H, Ar–H), 6.41 (s, 1H, CH); ^{13}C NMR (100 MHz), ppm: 165.46 (C=O), 164.71, 152.27, 139.29, 131.97, 130.14, 128.74, 127.96, 123.95, 123.77, 117.95, 115.99, 103.92 (CH), 35.71 (C-S Junction); LC-MS: *m/z* 401.17 [M^+]; $C_{22}H_{15}N_3O_3S$; Calculated, %: C, 68.32; H, 3.90; N, 9.56; O, 10.92; S, 7.30; Found, %: C, 68.41; H, 3.85; N, 9.52; O, 10.91; S, 7.31.

3-(((Benzo[*d*]imidazole-2yl)thio)(3-methylthiophen-2-yl)methyl)-4-hydroxynaphthalen-2(1*H*)-one (IVd). Green solid, yield: 92%, mp 28–130°C; FT-IR (KBr) ν_{max}, cm^{-1}: 3413.31 (–OH), 3081.10 (N–H), 2925.20 (Ar–H), 1668.18 (C=O), 1563.97 (C=N), 1447.63 (C=C), 760.21 (C–S), ^{1}H NMR (400 MHz, DMSO-d_6), ppm: 9.86 (s, 1H, NH, 7.90–7.26 (m, 8H, Ar–H), 6.99–6.35 (d, 3H, J = 5.6Hz, Ar–H), 5.60 (s, 1H, CH), 2.11 (m, 3H, CH_3); LC-MS: *m/z* 420.70 [M^+]; $C_{22}H_{16}N_2O_3S_2$; Calculated, %: C, 68.32; H, 3.90; N, 9.56; O, 10.92; S, 7.30; Found, % C, 68.36; H, 3.94; N, 9.50; O, 10.88; S, 7.32.

3-(((Benzo[*d*]imidazole-2yl)thio)(thiophen-2-yl)-methyl)-4-hydroxynaphthalen-2(1*H*)-one (IVe). Green solid, yield: 86%, mp 132–134°C; FT-IR (KBr) ν_{max}, cm^{-1}: 3428.86 (–OH), 3077.82 (N–H), 2982.22 (Ar–H), 1672.52 (C=O), 1577.31 (C=N), 1475.59 (C=C), 770.80 (C–S); ^{1}H NMR (400 MHz, DMSO-d_6), ppm; 10.14 (s, 1H, NH), 7.90–7.32 (m, 7H, Ar–H), 7.29–6.89 (m, 4H, Ar–H), 5.56 (s, 1H, CH); ^{13}C NMR (100 MHz, DMSO-d_6), ppm; 166.74 (C=O), 164.82, 152.82, 146.60, 132.30, 126.89, 124.24, 119.01, 116.36, 104.72, 33.30 (C–S Junction); LC-MS: *m/z* 406.47 [M^+]; Calculated, %: C, 68.32; H, 3.90; N, 9.56; O, 10.92; S, 7.30; Found, %: C, 68.38; H, 3.87; N, 9.60; O, 10.88; S, 7.27.

3-(((Benzo[*d*]imidazole-2yl)thio)(furon-2-yl)-methyl)-4-hydroxynaphthalen-2(1*H*)-one (IVf). Black solid; yield: 89%, mp 118–120°C; FT-IR (KBr) ν_{max}, cm^{-1}: 3441.12 (–OH), 3094.48 (NH), 2980.49 (Ar–CH), 1676.28 (C=O), 1557.56 (C=N), 1471.78 (C=C), 779.88 (C–S); ^{1}H NMR (400 MHz, DMSO-d_6), ppm: 12.43 (s, 1H, NH), 7.82–7.22 (m, 7H, Ar–CH), 7.18–6.96 (m, 4H, Ar–CH), 5.56 (s, 1H, CH); ^{13}C NMR (100 MHz, DMSO-d_6), ppm: 161.27 (C=O), 131.29, 124.16, 123.70, 123.14, 123.08, 115.65, 115.55, 115.42, 103.72, 34.85 (C–S Junction); LC-MS: *m/z* 389.20 [M^+]; $C_{21}H_{14}N_2O_4S$; Calculated, %: C, 68.32; H, 3.90; N, 9.56; O, 10.92; S, 7.30; Found, %: C, 68.29; H, 3.93; N, 9.53; O, 10.92; S, 7.33.

Biological activity. Sample preparation. The synthesized compounds (**IVa–IVf**) were tested cytotoxicity

against HeLa cells associated with their Acetyl CoA inhibitory activity in 10 to 50 μg/mL concentrations. HeLa cells were grown for 24 h at OD 1.2 and treated with the above listed compound further cells were centrifuged and washed with PBS buffer and cells were sonicated and further centrifuged for 10.000 rpm. The supernatant was used for the enzyme assay.

Acetylcholinesterase enzyme assay. The enzyme assay was carried out for ACAS reaction, the following reagents were combined in a 1 mL reaction volume: 50 mM acetyl-coA assay buffer, and acetyl-CoA synthetase along with the containing sample. The control reaction contained all of the components of the reaction, except acetyl-CoA synthetase. Following incubation at 37°C for 20 min, the reaction was terminated and 380 μL of supernatant was transferred to a test tube 50 μL of 2.5% molybdate reagent, 50 μL of 0.5 M 2-mercaptoethanol and 20 μL of Eikonogen was added for a total volume of 0.5 mL. At equilibrating for 10 min, the absorbance at 580 nm was determined using a plate reader (multiplate reader). The blank was prepared by similar treatment of the samples except that the samples were denatured before being added. The amount of PPi attributed to the action of acetyl-CoA synthetase was determined by subtracting the background absorbance at 580 nm measured in the control reaction with the absence of enzyme [48]. The formula used to determine the concentration is given below:

$$\text{Inhibitory activity} = \frac{A_s}{A_c} \times 100,$$

where A_s = Absorbance sample, A_c = absorbance control.

Antioxidant studies. The antioxidant activity of synthesized compounds was assessed using the modified DPPH 2,2-diphenyl-1-picryl-hydrazyl method. A sample was prepared 25 μL makeup to 600 μL with methanol and 200μL of 0.004% DPPH solution (4 mg DPPH in 100 mL MeOH) was added, further, it was incubated for 30 min in the dark medium. UV-absorbance was recorded at 517 nm in a UV-Vis spectrophotometer, and methanol was used as a blank solution. The experiment was conducted under dark conditions due to DPPH being extremely sensitive. The percentage of antioxidants was calculated by using the formula:

$$\text{RSA} = \frac{A_c - A_s}{A_c} \times 100.$$

Molecular docking studies. In order to understand how to target ligands and interact with appropriate receptors, the pharmacological activity of the generated compounds (**IVa–IVf**) was examined *in silico* molecular docking experiments. By using the method in Gaussian 09W software's energy minimization (optimizations), the stable structure of the produced molecules (ligands) was found, and the structures were then transferred into PDB format. The receptor for acetylcholinesterase, 1W6R, was selected and obtained from the Research Collaboratory for Structural Bioinformatics Protein Data Bank (RCSB PDB). The protein was prepared for docking experiments using the Pymol visualization program by eliminating water molecules, organic residues, and chains. Ligand (PDBQT), receptor (PDBQT), and grid box dimensions are created using the AutoDock tool. These pdbqt files were used for docking analysis in the AutoDock Vina program [49, 50] and for visualizing the results in the Discovery studio program and Chimera software [51–53]. The ligands' binding affinity and hydrophobic interactions with the binding site and protein surface were investigated.

CONCLUSIONS

In conclusion through one pot synthesis, we successfully designed and synthesized a novel series of coumarin-benzimidazole derivatives in the presence of an L-proline catalyst. FT-IR, ^{1}H NMR and ^{13}C NMR, LC-MS, and spectroscopic techniques confirm the structures of synthesized compounds. Computational investigations are performed to obtain optimized structures of synthesized molecules, global parameters and to calculate theoretical IR and NMR for comparative studies with the experimental data. In MEP analysis positive electrostatic potential was observed around the NH-group of the imidazole ring and negative electrostatic potential was observed around the carbonyl group of the coumarin ring. The smaller energy gap ranged from 3.23 to 4.23 eV, supported intermolecular electron transfer in molecules and their electrophilicity index was found in the range of 3.65 to 5.12 eV. The molecule's NLO powerful nature

is demonstrated by the nonlinear optical studies, and hyperpolarizability (β_0) values, which are seven times higher than those of urea. Furthermore, to investigate thermodynamic properties such as the compound's heat capacity, entropy and enthalpy to study the temperature depending nature of substances from correlation graphs. The drug likeness characteristics support the notion the target molecules are important from a pharmacological perspective. The synthesized compounds show promising bioactivity for the acetylcholine esterase enzyme. Among all, compound (**IVa**) exhibits good inhibition against Hela cancer cell lines which is also supported by the *in silico* docking studies in which (**IVa**) compound gives a good binding affinity of –10.1kcl/mol which indicates the best binding interactions compared to the target molecules with the receptor.

ACKNOWLEDGMENTS

The authors are sincerely thankful to the Chairman Department of Industrial Chemistry, Kuvempu University, Shimoga for the laboratory facility, and we are grateful to SAIF Mangalore University for spectral characterizations.

FUNDING

This work was supported by the University SC/ST cell and no additional grants were obtained.

ETHICS APPROVAL AND CONSENT TO PARTICIPATE

This article does not contain any studies involving patients or animals as test objects.

Informed consent was not required for this article.

CONFLICT OF INTEREST

No conflict of interest was declared by the authors.

AUTHOR CONTRIBUTION

The author MNTH—methodology, investigation, writing-original draft. The author IP—investigation, supervision, review, editing, DFT study, and docking analysis. The author P—contributed to the manuscript preparation. The author NYR—biological activity test.

SUPPLEMENTARY INFORMATION

The online version contains supplementary material available at https://doi.org/10.1134/S1068162024010229

DATA AVAILABILITY

The data that support the findings of this study are available from the corresponding author upon reasonable request.

REFERENCES

1. Sinha, S., Singh, K., Ved, A., Hasan, S.M., and Mujeeb, S., *Mini-Rev. Med. Chem.*, 2022, vol. 22, pp. 1314–1330. https://doi.org/10.2174/1389557521666211116120823
2. Kumar, K.A., Renuka, N., Pavithra, G., and Kumar. G.V., *J. Chem. Pharm. Res.*, 2015, vol. 7, pp. 67–81. https://eprints.uni-mysore.ac.in/id/eprint/5522
3. Qin, H.L., Zhang, Z.W., Ravindar, L., and Rakesh, K.P., *Eur. J. Med. Chem.*, 2020, vol. 207, Article ID: 112832. https://doi.org/10.1016/j.ejmech.2020.112832
4. Lončarić, M., Gašo-Sokač, D., Jokić, S., and Molnar, M., *Biomolecules*, 2020, vol. 10, p. 151. https://doi.org/10.1016/j.ejmech.2020.112832
5. Aras, A., *J. Indian Chem. Soc.*, 2022, vol. 99, Article ID: 100553. https://doi.org/10.1016/j.jics.2022.100553
6. Rajanarendar, E., Govardhan Reddy, K., Rama Krishna, S., Shireesha, B., Reddy, Y.N., and Rajam, M.V., *Med. Chem. Res.*, 2013, vol. 22, pp. 6143–6153. https://doi.org/10.1007/s00044-013-0598-0
7. Gaba, M., Singh, S., and Mohan, C., *Eur. J. Med. Chem.*, 2014, vol. 76, pp. 494–505. https://doi.org/10.1016/j.ejmech.2014.01.030
8. Araniti, F., Mancuso, R., Lupini, A., Giofrè, S.V., Sunseri, F., Gabriele, B., and Abenavoli, M.R., *Molecules*, 2015, vol. 20, pp. 17883–17902. https://doi.org/10.3390/molecules201017883
9. Dokla, E.M., Abutaleb, N.S., Milik, S.N., Kandil, E.A., Qassem, O.M., Elgammal. Y., and Adel. M., *Eur. J. Med. Chem.*, 2023, vol. 247, Article ID: 115040. https://doi.org/10.1016/j.ejmech.2022.115040
10. Ghirga, F., Quaglio, D., Mori, M., Cammarone, S., Iazzetti, A., Goggiamani, A., and Calcaterra, A., *Org. Chem. Frontiers*, 2021, vol. 8, pp. 996–1025. https://doi.org/10.2139/ssrn.4002339
11. Zhang, R.R., Liu, J., Zhang, Y., Hou, M.Q., Zhang, M.Z., Zhou, F., and Zhang, W.H., *Eur. J. Med. Chem.*, 2016, vol. 116, pp. 76–83. https://doi.org/10.1016/j.ejmech.2016.03.069

12. Zhang, H.Z., Zhao, Z.L., and Zhou, C.H., *Eur. J. Med. Chem.*, 2018, vol. 144, pp. 444–492. https://doi.org/10.1016/j.ejmech.2017.12.044
13. Han, X., Luo, J., Wu, F., Hou, X., Yan, G., Zhou, M., and Li, R., *Eur. J. Med. Chem.*, 2016, vol. 114, pp. 232–243. https://doi.org/10.1016/j.ejmech.2016.01.035
14. Nisha, H., Dheeraj, B., Rupali, B.K., and Rekha, D.P., *World J. Pharm. Res.*, 2021, vol. 10, pp. 234–246. https://doi.org/10.17605/OSF.IO/8GNH2
15. Padhy, G.K., Panda, J., Raul, S.K., and Behera, A.K., *Bioint. Res. Appl. Chem.*, 2020, vol. 11, pp. 11562–11591. https://doi.org/10.33263/BRIAC114.1156211591
16. Obaiah, N., Bodke, Y.D., and Telkar, S., *ChemistrySelect*, 2020, vol. 5, pp. 178–184. https://doi.org/10.1002/slct.201903472
17. Satija, G., Sharma, B., Madan, A., Iqubal, A., Shaquiquzzaman, M., Akhter, M., and Alam, M.M., *J. Heterocyc. Chem.*, 2022, vol. 59, pp. 22–66. https://doi.org/10.1002/jhet.4355
18. Dziwornu, G.A., Coertzen, D., Leshabane, M., Korkor, C.M., Cloete, C.K., Njoroge, M., and Chibale, K., *J. Med. Chem.*, 2021, vol. 64, pp. 5198–5215. https://doi.org/10.1021/acs.jmedchem.1c00354
19. Haribabu, J., Garisetti, V., Malekshah, R.E., Srividya, S., Gayathri, D., Bhuvanesh, N., and Karvembu, R., *J. Mol. Struct.*, 2022, vol. 1250, Article ID: 131782. https://doi.org/10.1016/j.molstruc.2021.131782
20. Manjunatha, B., Bodke, Y.D., Nagaraja, O., Nagaraju, G., and Sridhar, M.A., *J. Mol. Struct.*, 2021, vol. 1246, Article ID: 131170. https://doi.org/10.1016/j.molstruc.2021.131170
21. Frisch, M.J., Trucks, G.W., and Fox D.J., Gaussian 09, RevisionE. 01, Gaussian, Inc., Wallingford CT (2009).
22. Roy, D., Dennington II, Keith T.A., and John, M., Millam2016GaussView 6.0.16 (64-bit W) Semichem, Inc. 2000.
23. Lu, Y., Lan, Z., and Thiel, W., *J. Computat. Chem.*, 2012, vol. 33, pp. 1225–1235. https://doi.org/10.1002/jcc.22952
24. Lewis, D.F.V., Ioannides, C., and Parke, D.V., *Xenobiotica*, 1994, vol. 24, pp. 5401–408. https://doi.org/10.3109/00498259409043243
25. Al-Ostoot, F.H., Geetha, D.V., Mohammed, Y.H.E., Akhileshwari, P., Sridhar, M.A., and Khanum, S.A., *J. Mol. Struct.*, 2020, vol. 1202, p. 127244. https://doi.org/10.3109/00498259409043243
26. Gad, E.A., Azzam, E.M.S., and Halim, S.A., *Egyptian J. Petroleum*, 2018, vol. 27, pp. 695–699. https://doi.org/10.1016/j.ejpe.2017.10.005
27. Pushpavathi, I., Pasha, K.M., Muthu, S., and Amshumali, M.K., *Bull. Pure Appl. Sci. Chem.*, 2019, pp. 40–59. https://doi.org/10.48165
28. George, J., Prasana, J.C., Muthu, S., Kuruvilla, T.K., Savanthi, S., and Saji, R.S., *J. Mol. Struct.*, 2018, vol. 1171, pp. 268–278. https://doi.org/10.1016/j.molstruc.2018.05.106
29. Saral, A., Sudha, P., Muthu, S., Sevvanthi, S., Sangeetha, P., and Selvakumari, S., *Heliyon*., 2021, vol. 7, p. e07529. https://doi.org/10.48165
30. Muttannavar, V., Melavanki, R.M., Bhavya, P., Kusanur, R., Patil, N.R., and Naik, L.R., *Life Sci. Pharma Res*., 2018, vol. 3, pp. 24–30. https://doi.org/10.22376/ijpbs/lpr.2018.8.3.L24-30
31. Shiroudi, A., Safaei, Z., Kazeminejad, Z., Repo, E., and Pourshamsian, K., *J. Mol. Modeling*, 2020, vol. 26, pp. 1–11. https://doi.org/10.1007/s00894-020-4316-9
32. Miar, M., Shiroudi, A., Pourshamsian, K., Oliaey, A.R., and Hatamjafari, F., *J. Chem. Res.*, 2021, vol. 4, pp. 147–158. https://doi.org/10.1177/1747519820932091
33. Ignov, S.K., *Program Mol. Visualizat. Thermodynam. Calculat.*, 2004.
34. Zhang, R., Du, B., Sun, G., and Sun, Y.X., *Spectrochim. Acta A*, 2010, vol. 75, pp. 1115–1124. https://doi.org/10.1016/j.saa.2009.12.067
35. Rajamani, T., Muthu, S., and Karabacak, M., *Mol. Biomol. Spectr.*, 2013, vol. 108, pp. 186–196. https://doi.org/10.1016/j.saa.2013.01.090
36. Kecel-Gunduz, S., Budama-Kilinc, Y., Bicak, B., Gok, B., Belmen, B., Aydogan, F., and Yolacan, C., *Arabian J. Chem.*, 2023, vol. 16, Article ID: 104440. https://doi.org/10.1016/j.arabjc.2022.104440
37. Aryal, S., Baniya, M.K., Danekhu, K., Kunwar, P., Gurung, R., and Koirala, N., *Nepal. Plants*, 2019, vol. 8, p. 96. https://doi.org/10.3390/plants8040096

38. Rakesh, B., Bindu, K.H., and Praveen, *Asian J Chem.*, 2021, vol. 33, pp. 1881–1890.
39. Lipinski, C.A., Lombardo, F., Dominy, B.W., and Feeney, P.J., *Drug. Delivery Rev.*, 1997, pp. 4–17. https://doi.org/10.1016/j.addr.2012.09.019
40. Veber, D.F., Johnson, S.R., Cheng, H.Y., Smith, B.R., Ward, K.W., and Kopple, K.D., *J. Med. Chem.*, 2002, vol. 45, pp. 2615–2623. https://doi.org/10.1021/jm020017n
41. Ali, J., Camilleri, P., Brown, M.B., Hutt, A.J., and Kirton, S.B., *J. Chem. Inf. Modell.*, 2012, vol. 52, pp. 420–428. https://doi.org/10.1021/ci200387c
42. Husain, A., Ahmad, A., Khan, S.A., Asif, M., Bhutani, R., and Al-Abbasi, F.A., *Saudi Pharm. J.*, 2016, vol. 24. pp. 104–114. https://doi.org/10.1016/j.jsps.2015.02.008
43. Rahuman, M.H., Muthu, S., Raajaraman, B.R., Raja, M., and Umamahesvari, H., *Heliyon.*, 2020, vol. 6, Article ID: e04976. https://doi.org/10.1016/j.heliyon.2020.e04976
44. Wezhli, M.M., Balamurugan, P., Raju, K., Sevvanthi, S., Irfan, A., Javed, S., and Muthu, S., *J. Mol. Struct.*, 2023, vol. 12741, Article ID: 34324. https://doi.org/10.1016/j.molstruc.2022.134324
45. Maliyappa, M.R., Keshavayya, J., Sudhanva, M.S., and Pushpavathi, I., *J. Mol. Struct.*, 2022, vol. 1247, Article ID: 131321. https://doi.org/10.1016/j.molstruc.2021.131321
46. Fatima, A., Khanum, G., Agrawal, D.D., Srivastava, S.K., Butcher, R.J., Muthu, S., and Javed, S., *Polycyclic Aromatic Comp.*, 2023, vol. 43, pp. 4242–4270. https://doi.org/10.1080/10406638.2022.2089174
47. Trott, O. and Olson, A.J., *J. Computat. Chem.*, 2010, vol. 31, pp. 455–461. https://doi.org/10.1002/jcc.21334
48. Kuang, Y., Salem, N., Wang, F., Schomisch, S.J., Chandramouli, V., and Lee, Z.A., *J. Biochem. Biophys. Methods*, 2007, vol. 70, pp. 649–655. https://doi.org/10.1016/j.jbbm.2007.02.008
49. El-Sonbati, A.Z., Mohamed, G.G., El-Bindary, A.A., Hassan, W.M.I., Diab, M.A., Morgan, S.M., and Elkholy, A.K., *J. Mol. Liq.*, 2015, vol. 212, pp. 487–502. https://doi.org/10.1016/j.molliq.2015.09.038
50. Nagaraja, O. Bodke, Y.D., Pushpavathi, I., and Kumar, S.R., *Heliyon.*, 2020, vol. 6, Article ID: e04245. https://doi.org/10.1016/j.heliyon.2020.e04245
51. Pettersen, E.F., Goddard, T.D., Huang, C.C., Couch, G.S., Greenblatt, D.M., Meng, E.C., and Ferrin, T.E., *J. Computat. Chem.*, 2004, vol. 25, pp. 1605–1612. https://doi.org/10.1002/jcc.20084
52. Matada, M.N., Jathi, K., Malingappa, P., and Pushpavathi, I., *Chem. Data Collect.*, 2020, vol. 25, Article ID: 100314. https://doi.org/10.1016/j.cdc.2019.100314
53. Maliyappa, M.R., Keshavayya, J., Mallikarjuna, N.M., and Pushpavathi, I., *J. Mol. Struct.*, 2020, vol. 1205, Article ID: 127576. https://doi.org/10.1016/j.molstruc.2019.127576